2019-09-01

Effects of Infiltration Temperature, Time, and Gas Flow Rate on Material Properties of Carbon Infiltration Carbon Nanotubes

Shane Dirk Sypherd
Brigham Young University

Effects of Infiltration Temperature, Time, and Gas Flow Rate on Material Properties of Carbon Infiltrated Carbon Nanotubes

Shane Dirk Sypherd

A thesis submitted to the faculty of
Brigham Young University
in partial fulfillment of the requirements for the degree of

Master of Science

Brian D. Jensen, Chair
Eric R. Homer
Brian D. Iverson

Department of Mechanical Engineering

Brigham Young University

ABSTRACT

Effects of Infiltration Temperature, Time, and Gas Flow Rate on
Material Properties of Carbon Infiltrated Carbon Nanotubes

Shane Dirk Sypherd
Department of Mechanical Engineering, BYU
Master of Science

This work characterizes the material properties of carbon infiltrated carbon nanotube (CI-CNT) structures. The impacts of temperature, time, and hydrogen flow rates on the material properties of modulus of elasticity and strength are examined and compared. Carbon infiltration levels are assessed through the use of SEM images to determine which parameters give the highest level of infiltration. Through the use of SEM, carbon capping is observed on samples infiltrated for longer times at 900 and 950° C, suggesting that the samples are not being infiltrated during the entire desired infiltration period at these temperatures. The highest material properties of modulus and strength were reached when infiltrating the carbon nanotube forests for 150 mins at 850° C with hydrogen flowing at 311 sccm (0.0115 m/s). With these parameters, a modulus of 20.4 GPa and strength of 289.8 MPa were attained. The poorest results were seen when the samples were infiltrated at 800° C, and is therefore not recommended as an infiltration temperature if high modulus and strength are desired. Density is correlated to strength and modulus and it is seen that there is a strong correlation between higher strength and modulus with higher density.

Keywords: CI-CNT, carbon nanotubes, material properties, 3-point bend test

ACKNOWLEDGMENTS

Looking back upon completing my research I realize that I have many people to thank who made it all possible.

First, I would like to thank Dr. Brian Jensen for being my advisor and for all of the things that he has taught me over the last few years. I am also thankful for his understanding and patience as I worked through the experiment. I would also like to thank Dr. Brian Iverson and Dr. Eric Homer for being on my committee and for their input along the way.

I would like to thank Andrew Cunningham for his countless hours taking SEM images and for helping with nanotube growths, as well as Daniel Snow and Fred Fagergren for their help in the lab. I would like to thank Jason Lund for teaching me the ropes as well as training me on how to fabricate CNTs, use all of the machines, and use the furnace. Thank you to the physics and electrical engineering departments for the generous use of their facilities in the fabrication process.

I would like to thank my wife, Ariel, for her support and words of motivation throughout the whole process. I would also like to thank Brigham Young University and Tag Heuer for their funding of the research.

TABLE OF CONTENTS

LIST OF TABLES

LIST OF FIGURES

CHAPTER 1. INTRODUCTION

1.1 Background

In the microelectromechanical systems (MEMS) field many devices use compliant mechanisms, rather than rigid links and joints, to achieve their motion. It has been shown that carbon infiltrated carbon nanotubes (CI-CNTs) can achieve such motion on the micro scale and have many advantages when it comes to their material selection. Advantages include the ability to pattern and grow CI-CNTs for precise geometry, as demonstrated by Hutchison et al. [1], good thermal properties, biocompatibility [2], and reasonable strength. Toone et al. demonstrated these advantages in their work with cell restraint CNT MEMS [3].

One advantage with CI-CNTs is that the material is capable of variation in material properties by varying growth and infiltration parameters. However, the specific effects of these parameters are not well understood. The proposed research aims to quantify the effects of gas flow rates, temperatures, and times during the carbon infiltration stage of CI-CNT production on the CI-CNT structure's modulus of elasticity and strength. With better material characterization and optimized manufacturing conditions, the aim is to be able to better predict the performance of CI-CNT devices.

1.2 Previous Works

There has been a good deal of work already on the subject of carbon nanotubes. Qian et al. measured the mechanical properties of single and multi wall carbon nanotubes and found that the tensile strength of the outermost shell of MWCNTs can be 100 times greater than that of aluminum [4]. There has also been a good deal of work done measuring the electrical properties of carbon nanotubes. Zhao et al. showed that nanotubes can be infiltrated with many different substances such as polymers, which can change the electrical and mechanical properties of the

nanotube structures. They infiltrated the grown nanotube forests by sonicating their samples in polymer solutions. They found that sonicating helped, but still did not provide for complete infiltration of the nanotubes [5]. Ding et al. used vertically aligned carbon nanotubes on PDMS to demonstrate the possible use of nanotubes for flexible electronics such as displays, energy devices, and wearable sensors [6]. Lee et al. measured the electrical properties of thin film polymers with nanotubes randomly deposited in them for use as nanocomposite strain sensors [7]. Lee et al. developed single walled carbon nanotube film strain gauges with possible applications such as highly sensitive strain, weight, or pressure sensors on the macro-scale [8]. Robinson and Jones created coronary stents using patterned CI-CNT forests [9] [10]. Stevens et al. demonstrated the ability to use CI-CNTs as hydrophobic surfaces with tunable geometry [11]. Lawrence et al. studied the material properties of nickel infiltrated carbon nanotubes infiltrated through electroplating CNT structures [12]. Wang et al. investigated the influences of adding carbon nanotubes to carbon fiber/silicon carbide (Cf/SiC) composites [13]. Li et al. used self-supporting and flexible activated carbon/carbon nanotube/reduced graphene oxide (AC/CNT/RGO) to construct high-performance supercapacitors [14].

This research focuses on CI-CNTs which are infiltrated using Chemical Vapor Deposition (CVD) [15], which have in past research had a problem with incomplete infiltration. The extent of this infiltration problem will be evaluated in this research.

There has not, however, been much done on the subject of CI-CNTs and their mechanical properties. Previous studies have measured modulus and maximum strain using cantilevered CI-CNTs. In Fazio et al's work the stresses were applied to the nanotubes perpendicular to the direction of their growth with the nanotubes oriented vertically. The data was run through a finite element analysis in ANSYS due to the large deflections [16]. This research uses a three-point bending test with a small gap the beam has to span in order to keep the beam bending in the small deflection range. This helped to avoid large deflections and allowed for the use of small deflection approximation equations. Stresses were applied to the nanotubes perpendicular to the direction of their growth with the nanotubes oriented horizontally. This orientation matches the loading found in most MEMS.

Hanna et al. measured ultimate strength, modulus, and maximum strain of CI-CNTs with stresses applied in the direction parallel to CNT growth using a 3-point bending test [17]. This

research measures the CNTs in their horizontal direction and allows for comparison to these results and demonstrates the difference in material properties when loaded in different directions.

1.3 Thesis Objective

For this research project 144 samples were prepared and grown in order to do a full factorial experiment. There were four different infiltration times (10 min, 25 min, 45 min, 70 min), four different infiltration temperatures (800, 850, 900, 950° C), and three different hydrogen flow rates (311 sccm, 396.5 sccm, 492.4 sccm). Each of the 48 different factor combinations had three replicates, giving us 144 total samples to fabricate. Each of the samples had 25 patterned beams of 0.2 mm width and 6 mm length. The desired height of the beams was between 300 and 425 microns [18], which was controlled by the growth time of the nanotubes in the tube furnace. The height is difficult to control and is the reason for the wide interval of desired height. We grew so many beams per sample to be able to get 10 good beams off of the substrate and through the entire testing process. To do this, 12 beams were removed from the substrate and put through the testing process with the realization that some of the beams were likely to break in the measuring and handling process. Removal of nanotubes from their substrate can be difficult. This was demonstrated by Robinson who attempted to remove coronary stents from convex cylindrical substrates using dry etching, a wet KOH bath, wet etching in HCL, and thermal shock with little success using any of the methods to remove the nanotubes from their substrates [9]. The method used for removal of CI-CNTs from their substrates that was used in this research was through manual physical removal of the CI-CNT beams using a razorblade to effectively pop the nanotubes off their substrate. This method does cause some beams to break in the removal process and is the main reason for having 25 patterned, grown, and infiltrated beams on each sample to allow for this problem. For this experiment the testing process included:

- Removing 12 whole CI-CNT beams from their substrate in good condition. This was done by hand with a razorblade.
- Weighing each batch of 12 beams. The weight was used to calculate the density of each set of beams. This was done with a high precision scale furnished by the chemistry department at BYU as the nanotube beams weigh very little.

- Measuring both the height and width of each beam individually. These measurements were used in the calculations of both density as well as modulus. This was done using a Keyence digital microscope zoomed in to 300x magnification.

- 3-point bend testing each beam individually which was used to calculate modulus and strength. This was done on a mini Instron using a one pound load cell for precise measurement. It was done using a custom-made fixture with a 3.2 mm gap and a razorblade attached to the load cell.

- SEM images of one beam from one of the three replicates of each factor combination. The SEM was used to measure diameters of nanotubes at top and bottom of sample to see to what extent the nanotubes were infiltrated. It also looked at the top of the beam sample to see if it has been capped or completely coated, and therefore not allowing further infiltration to occur.

The data that was collected throughout the testing process was analyzed graphically and statistically to see what parameters cause significant differences in the CI-CNT material properties.

The main purpose of this research was to characterize material properties of CI-CNTs, especially when loaded in the direction perpendicular to their growth with the nanotubes oriented horizontally. This is of value in order to aid in more accurate design and development of CI-CNT MEMS devices.

CHAPTER 2. CI-CNT MATERIAL PROPERTIES EXPERIMENT

2.1 Experimental Methods

Fabrication of the CI-CNTs followed the same general procedure as Fazio [19], with necessary modifications. The process is described below and can be seen in Figure 2.1.

2.1.1 Wafer Preparation

A 4 inch (100) silicon wafer was patterned using AZ-3312 positive photoresist using standard photolithography procedures (step (a) of Figure 2.1). A single project specific mask was designed and manufactured to pattern small beams that were 0.2 mm wide and 6 mm long. After the wafer was patterned and developed using MIF300, a 40 nm layer of alumina (Al_2O_3) was deposited using an electron beam evaporator (step (b) of Figure 2.1). The alumina acts as a buffer between the iron layer, which was deposited afterwards, and the silicon wafer, to prevent diffusion of the iron into the silicon at elevated growth temperatures. A 4 nm layer of iron was then deposited on top of the alumina layer using a thermal evaporator (step (c) of Figure 2.1) [20]. The iron acts as the catalyst in the CNT growth.

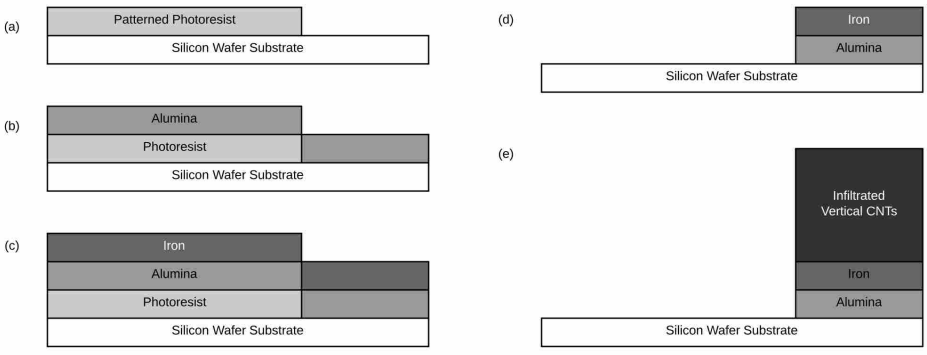

Figure 2.1: Sample Preparation Process

The final patterned samples were obtained through liftoff of the wafer in a sonicated bath of NMP (N-Methyl-2-pyrrolidone) to remove the remaining photoresist (Step (d) of Figure 2.1). Another layer of photoresist was then applied to act as a protective coating as the wafer was cut into smaller pieces that could fit into a 1 inch tube furnace, using a diamond dicing wheel and dicing saw. The top layer of photoresist was then removed to leave the diced pieces clean and ready for CNT growth.

2.1.2 Carbon Nanotube Growth

Chemical vapor deposition (CVD) was used to grow and infiltrate the CI-CNTs. The nanotubes were grown by inserting a patterned sample on a quartz boat into a tube furnace using a 24 mm inner diameter quartz tube. The tube was heated to 750° C with argon flowing in the tube. At 750° C, hydrogen at 311 sccm (0.0115 m/s) was allowed to flow, then the argon was turned off, and ethylene (C_2H_4) at 338 sccm (0.0125 m/s) was turned on for 5 mins and 30 seconds to grow the nanotubes. After the growth time, the ethylene was turned off, argon was turned on, and hydrogen was turned off at which time the temperature was increased to the desired temperature for infiltration (step (e) of Figure 2.1).

2.1.3 Carbon Nanotube Infiltration

Up to this point the samples had all been prepared using the same process. The designed experiment changed the parameters of infiltration to see how these changes affect the CI-CNT material properties. The full factorial experiment, requiring 144 samples to get 3 replicates of each combination, was designed to change temperature, hydrogen flow rate, and time during infiltration. The temperatures used were 800, 850, 900, and 950° C. The hydrogen flow rates used were 311 sccm (0.0115 m/s), 396.5 sccm (0.0146 m/s), and 492.4 sccm (0.0181 m/s). The times used were 10, 25, 45, and 75 mins. The growth and infiltration order of the 144 samples was randomized to avoid bias as much as possible during the experiment. This randomization helped to remove bias during sample preparation by randomizing the effects of variation in alumina and iron thickness from the electron beam evaporator and thermal evaporator. It also removed bias in growth

and infiltration both in furnace variation and human variation in who performed the growth and infiltration.

After growth the furnace was heated to the correct infiltration temperature for the sample being prepared. The hydrogen was then set at the correct flow rate and was let to flow in the tube. Argon was then turned off and ethylene was then allowed to flow in the tube at the same 338 sccm (0.0125 m/s) it was during growth. The sample was then left in this state to be infiltrated for the specified time for each particular sample. After the correct time had elapsed the ethylene was turned off, the argon was turned on, and then the hydrogen was turned off and the furnace was opened and allowed to cool down to a temperature that allowed the sample to be removed.

2.2 CI-CNT Measurements

2.2.1 Beam Removal from Substrate

A razor blade was used to remove the infiltrated beams from their silicon substrates. This was done by placing the razor blade against the substrate and carefully pushing the blade against the base of the CI-CNT beam. Twelve of the released beams were then gathered to be weighed. The experiment called for 10 beams to be used in testing, so 12 beams were gathered to account for some beams likely being accidentally broken in transport and measuring. Figure 2.2 shows a sample with several beams already removed.

2.2.2 Weight, Dimension, and Density

The 12 beams were then measured using a high precision digital scale accurate to 0.0001 grams. After being weighed the lengths of the beam's heights and widths were measured using a Keyence digital microscope. The beams were patterned to be 6 mm long and with the width, height, and weight measurements, the average density of the beams was calculated.

2.2.3 SEM Imaging

One beam of each of the different infiltration parameter combinations was imaged using a scanning electron microscope. The CI-CNT beam was cut with a razor blade and imaged on

Figure 2.2: Grown and infiltrated carbon-nanotube beam structures with some beams already removed.

the top and in the middle to see how deep the structures were infiltrated with carbon and to see if capping, or complete infiltration, had occurred on the surface. Knowing if the beams were capped was of interest because if the top is completely closed off or capped, then the carbon can no longer reach the lower part of the CI-CNT beam structure.

2.2.4 3-Point Bending Test

A Mini Instron was then used to 3-point bend test each beam. A custom stage with a 3.2 mm gap was fabricated as well as a custom apparatus to attach a razor blade to a one pound load cell. Each beam was tested by using tweezers to place it over the 3.2 mm gap in the center of the stage where the razor blade would come down and break it, as seen in Figure 2.3. The beam was placed over the gap so that it was simply supported on each side, and therefore allowed to move freely during the bending test.

A program was written within the Instron software package to gather the force and deflection data from each test. The CI-CNT beams were oriented on the stage with the nanotubes running

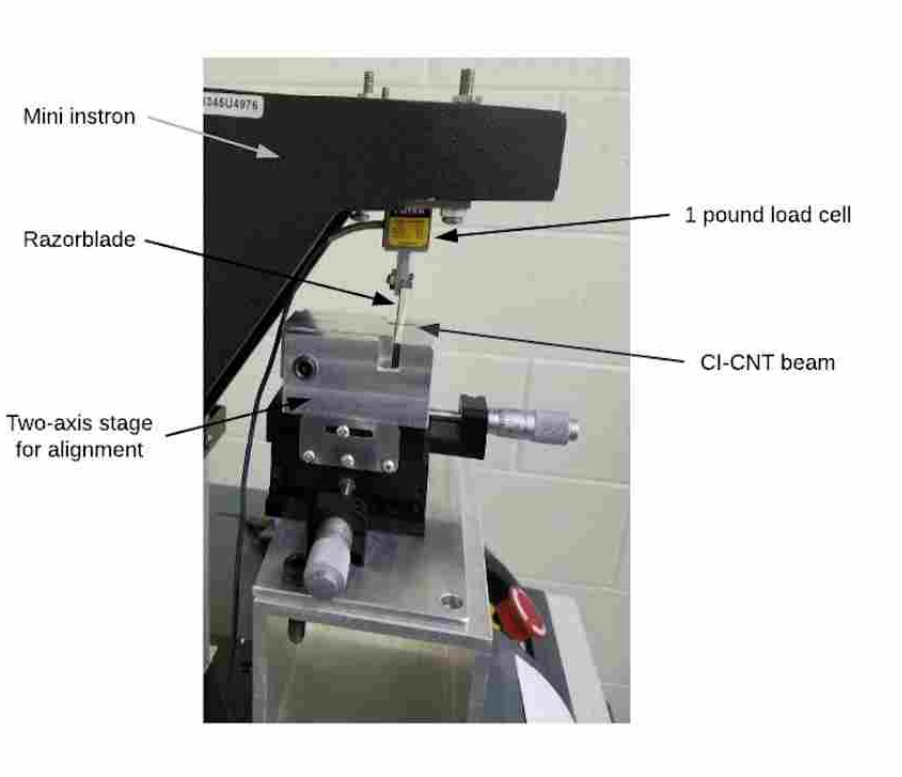

Figure 2.3: Mini Instron setup for 3-point bending tests

parallel to the direction of the razor blade, as seen in Figure 2.4. This orientation was desirable because there are no know documented experiments of testing CI-CNT structures in this orientation, which is the orientation in which CI-CNT structures and devices in MEMS applications are typically loaded.

2.2.5 Data Extraction

A python program was written to take the collected data and cut it down to a usable form by removing the data before the razor blade was touching the beam and after the beam was broken. A typical set of force-deflection curves can be seen in Figure 2.5. From the useable data, the slope of the force-deflection curve, or stiffness, was found and together with the geometry measurements taken earlier the bending strength and modulus were calculated. MATLAB was used to plot the average strength and modulus for each of the different infiltration parameter combinations to see the trends. The equation for calculating the modulus can be seen in Equation 2.1, where k is the stiffness, l is half the distance of the gap the beam spans, and I is the moment of inertia. The

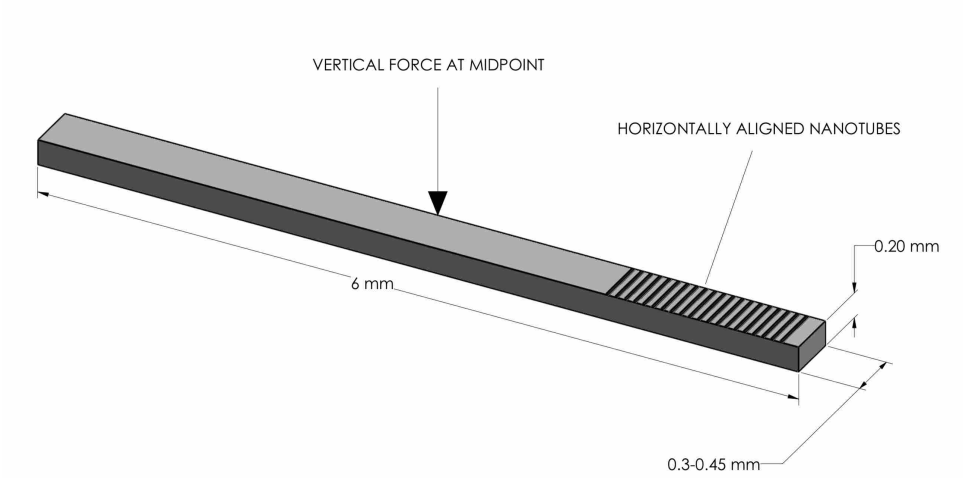

Figure 2.4: Orientation of beam for testing

equation for flexural strength can be seen in Equation 2.2, where F is the maximum force, c is the distance from the neutral axis to the outside of the beam, and I is the moment of inertia. The assumptions used for these equations to be valid were [21]:

- The beam is subjected to pure bending. This means that the shear force is zero, and no torsion or axial loads are present (for most engineering applications it is assumed that these loads affect the bending stresses minimally).
- The material is isotropic and homogeneous. Note that, for at least some samples in this experiment, the material is likely not homogeneous due to capping of the infiltrated carbon, leading to heavier carbon deposition on the outside of the beam. Hence, these equations result in an effective modulus for the material, representing an approximate average across the beam.
- The material obeys Hooke's law.
- The beam is initially straight with cross section that is constant throughout the beam length.
- The beam has an axis of symmetry in the plane of bending.

- The proportions of the beam are such that it would fail by bending rather than by crushing, wrinkling, or sideways buckling.
- Plane cross sections of the beam remain in plane during bending.

$$E = kl^3/48I \tag{2.1}$$

$$S = Flc/I \tag{2.2}$$

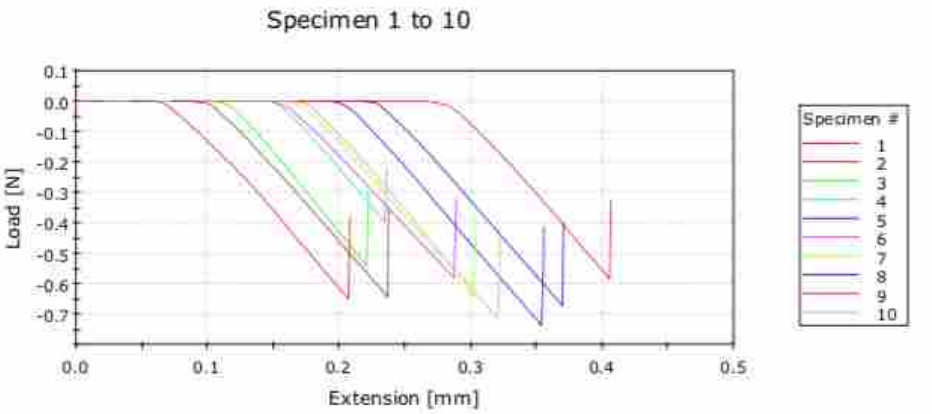

Figure 2.5: Set of typical Force vs Deflection Curves

2.3 Results and Discussion

Results of the experiment are shown graphically and explained in the next several sections.

2.3.1 3-Point Bend Test Results

Figure 2.6 shows the average modulus of elasticity for each of the distinct experiments described in the methods section. The 10 min infiltrations for all of the experiments at each different hydrogen flow rate at 800° C were removed from the data due to minimal infiltration causing the beams to not come cleanly off of the silicon substrate. The 70 min infiltrations for both the hydrogen flow rates of 311 sccm (0.0115 m/s) and 396.5 sccm (0.0146 m/s) were also removed due to false breakage readings observed from carbon flash breaking on the edges of the beams due to

Table 2.1: Full Results

Temp (ºC)	Flow Rate (sccm)	Time (min)	# of Beams	Avg Diameter of Nanotubes (nm)	Avg Modulus (GPa)	Modulus Std Dev (Gpa)	Avg Strength (Mpa)	Strength Std Dev (Mpa)	Avg Density (kg/m^3)	Density Std Dev (kg/m^3)
800	311	25	22	39.658	0.416	0.004	8.473	21.099	303.502	0.111
800	311	45	27	56.299	2.536	0.052	45.001	30.144	641.225	1.617
800	311	70	30	65.554	3.593	0.224	46.265	93.916	810.462	3.184
850	311	10	31	54.982	0.018	0.338	0.434	111.038	74.098	5.347
850	311	25	33	91.971	0.526	0.206	9.463	16.110	473.060	4.578
850	311	45	22	92.459	6.911	0.599	119.479	37.894	1158.493	18.528
850	311	70	32	134.396	3.908	3.090	21.911	65.070	659.737	78.789
900	311	10	35	78.490	0.120	1.170	3.577	91.916	202.143	21.910
900	311	25	34	110.929	3.863	1.743	70.490	125.172	978.172	46.113
900	311	45	33	107.787	6.580	1.400	98.456	51.104	1116.799	33.107
900	311	70	31	129.566	8.742	2.861	49.223	101.093	710.523	35.836
950	311	10	24	73.586	0.470	0.541	7.646	138.765	394.732	18.458
950	311	25	18	77.733	7.254	1.105	132.819	10.223	1198.410	6.803
950	311	45	19	70.198	8.626	2.987	110.458	24.759	1251.663	24.434
800	396.5	25	10	42.820	0.027	0.021	0.955	16.314	91.219	0.425
800	396.5	45	29	50.279	1.077	0.031	16.434	7.549	517.199	0.791
800	396.5	70	21	48.034	3.821	0.024	47.513	2.749	750.848	0.568
850	396.5	10	22	41.299	0.022	0.019	0.722	0.809	69.053	0.633
850	396.5	25	19	71.012	0.241	0.029	5.254	40.756	183.588	0.740
850	396.5	45	20	54.994	7.577	0.150	133.652	60.963	1175.424	5.970
850	396.5	70	33	106.638	4.960	0.405	34.889	65.834	763.428	16.261
900	396.5	10	26	50.539	0.053	1.058	1.662	138.926	132.401	13.946
900	396.5	25	21	111.993	1.157	2.915	20.769	55.608	687.768	84.840
900	396.5	45	35	125.610	7.607	2.385	161.157	48.593	1158.256	57.694
900	396.5	70	23	105.642	8.318	1.539	56.330	112.079	988.495	43.384
950	396.5	10	24	85.013	0.083	1.803	1.697	89.699	190.736	23.842
950	396.5	25	33	102.035	3.564	0.667	59.794	46.619	951.305	16.330
950	396.5	45	28	80.024	6.886	2.987	119.477	63.740	1244.882	32.440
800	492.4	25	24	79.151	0.017	0.007	0.685	18.598	77.111	0.284
800	492.4	45	32	45.074	0.451	0.020	8.907	10.675	454.420	0.606
800	492.4	70	22	34.843	3.249	0.100	40.953	46.886	818.181	1.575
850	492.4	10	18	40.605	0.008	0.009	0.385	13.707	47.699	0.480
850	492.4	25	22	52.106	0.112	0.069	3.050	83.208	220.285	2.122
850	492.4	45	22	62.176	2.325	2.832	46.298	361.343	847.382	41.459
850	492.4	70	35	91.922	4.558	0.506	53.444	39.751	891.267	10.400
900	492.4	10	27	65.838	0.033	0.203	1.055	86.481	101.052	3.609
900	492.4	25	22	115.822	0.246	0.569	3.908	111.648	334.426	17.866
900	492.4	45	31	82.294	5.854	1.585	109.283	30.635	1129.075	54.740
900	492.4	70	34	43.892	5.134	1.154	59.389	80.319	977.708	32.526
950	492.4	10	20	94.582	0.153	0.338	3.570	22.660	202.523	19.056
950	492.4	25	33	91.567	2.759	1.064	49.199	67.261	864.216	14.161
950	492.4	45	22	100.299	6.451	0.460	121.603	76.839	1257.115	16.343
950	492.4	70	22	121.315	10.522	2.740	89.744	29.310	1064.467	36.291
850	311	150	24	104.922	17.528	2.954	252.818	40.318	1278.010	64.011

high amounts of carbon deposition on the substrate. These data points were completely removed from the experiment and therefore will not be included in any subsequent charts or findings. These removed samples can be seen in Table 2.2. Table 2.1 shows the results of the entire experiment for each of the different parameters used.

Figure 2.6 shows an averaged chart of the modulus of elasticity vs time for each of the different temperatures and hydrogen flow rates. Each point represents the average of at least 20

Table 2.2: Experiment Design Highlighting the Samples
Removed from Consideration

Chart X3 for full experiment	INFILTRATION TIME (Min)				SCCM
INFILTRATION TEMP (C)	10	25	45	70	
800	N/A	2	3	4	
850	5	6	7	8	311
900	9	10	11	12	
950	13	14	15	N/A	
INFILTRATION TEMP (C)	10	25	45	70	
800	N/A	18	19	20	
850	21	22	23	24	396.5
900	25	26	27	28	
950	29	30	31	N/A	
INFILTRATION TEMP (C)	10	25	45	70	
800	N/A	34	35	36	
850	37	38	39	40	492.4
900	41	42	43	44	
950	45	46	47	48	

beams tested with their particular corresponding parameters. The CI-CNT beams infiltrated at 800° C for even long lengths of time (70 mins) have a very low modulus, never reaching even 1 GPa. There is a general trend of higher modulus of elasticity with longer infiltration times and lower hydrogen flow rates. The beams infiltrated at 850° C also seemed to be giving poor resulting modulus values in the beginning, but at longer times and lower hydrogen flow rates the modulus actually reached that of the beams infiltrated at 900 and 950° C. The data in Figure 2.6 also shows that the modulus of the beams infiltrated at 850° C are steadily increasing, and suggests that with more infiltration time these beams could reach the modulus values of the beams infiltrated at 900 and 950° C. Figure 2.7 shows the average strengths for the same data set used in Figure 2.6. Once again the figure shows that the beams infiltrated at 800° C for any amount of time have very low strength, and this coupled with their low modulus demonstrates that 800° C is likely not a good infiltration temperature for CI-CNT structures or devices that must demonstrate even small amounts of strength. We see a similar trend to that of modulus for the beams infiltrated at 850° C in that they are steadily increasing with time and at 70 mins at low hydrogen flow rates they actually surpass the strengths of the beams infiltrated for 70 mins at 900 and 950° C. This is likely due to capping of the outside of the CI-CNT beams infiltrated at 900 and 950° C, stopping the carbon from infiltrating deeper into the beams. In addition, the beams infiltrated at 900° C initially increase in strength with time, but they reach a maximum at about 100-140 MPa, suggesting that

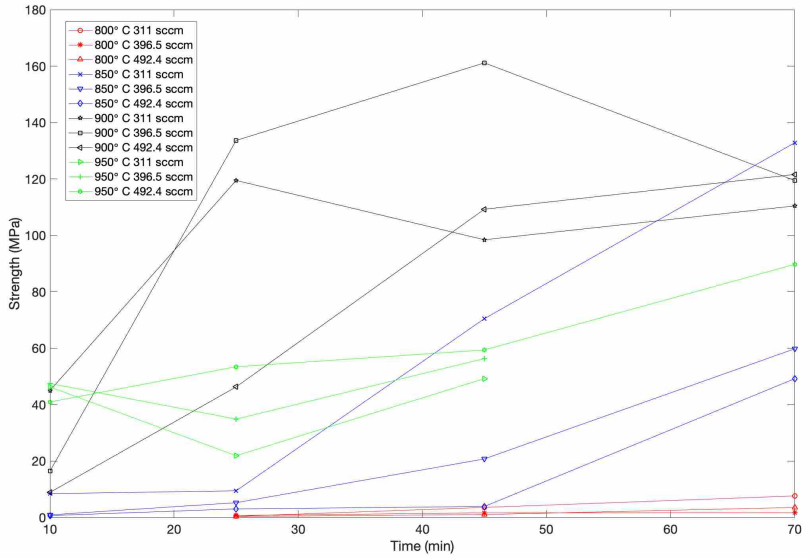

Figure 2.6: Modulus vs Time for full original experiment

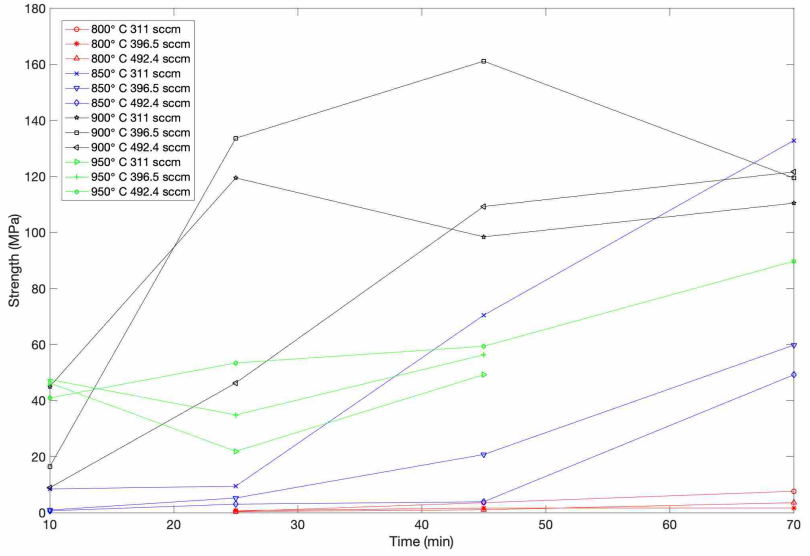

Figure 2.7: Strength vs Time for full original experiment

an outer cap has formed, preventing further infiltration of the interior of the beam. The beams infiltrated at 950° C also show this behavior, though the strength of these beams is generally lower than the 900° C beams. This suggests even more pronounced capping of the infiltration at higher temperatures.

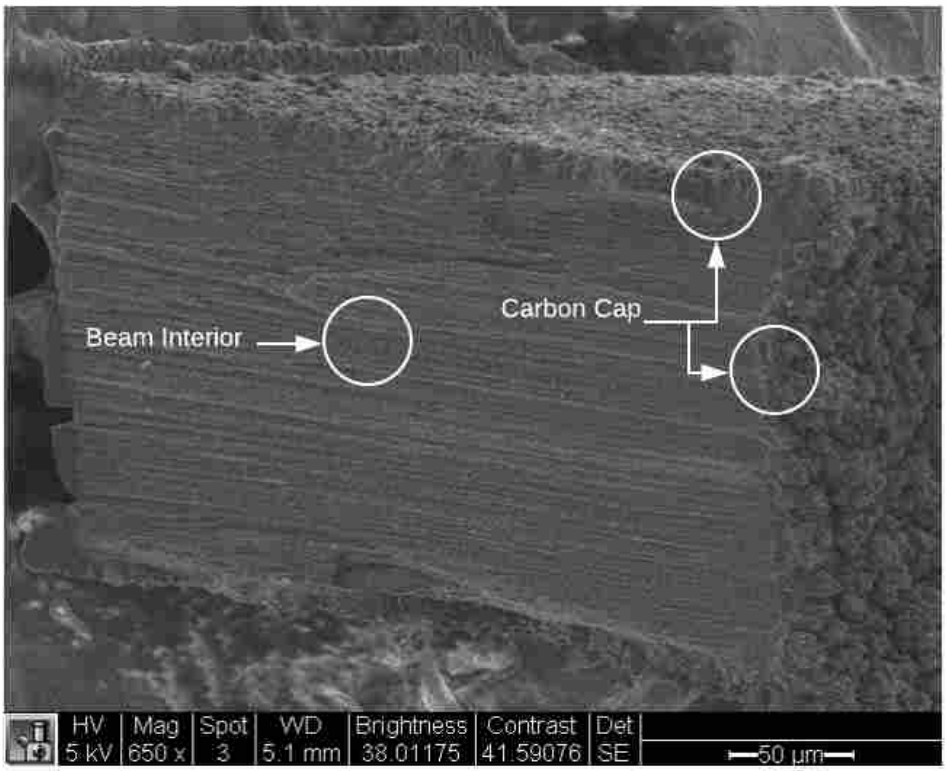

Figure 2.8: Capped CI-CNT Structure (Infiltrated for 45 mins at 950° C with hydrogen flowing at 311 sccm (0.0115 m/s)

2.3.2 SEM Imaging Results

Images taken with a scanning electron microscope of the broken beams gave insight into the hypothesis as to why the samples infiltrated at lower temperatures (850° C) were steadily increasing in both modulus of elasticity and in strength, while those infiltrated at 900 and 950° C did not have the same increasing relationship. In Figure 2.8 there is visible capping, or buildup of carbon on the surface of the nanotube beam. This capping is believed to be the result of quick infiltration with carbon particles that in effect clog or cap off the nanotubes not allowing any further infiltration into the center of the beam structures. This beam was infiltrated for 45 mins at 950° C with hydrogen flowing at 311 sccm (0.0115 m/s). Figure 2.9 shows a nanotube beam infiltrated with the same parameters of 45 mins with hydrogen flowing at 311 sccm (0.0115 m/s), but at only 850° C. The beam in Figure 2.9 does not have this same carbon capping or build up.

Looking closer into these same images near the bottom of the structures (the left side of the cross section in both images), or near where they were attached to the silicon substrate before

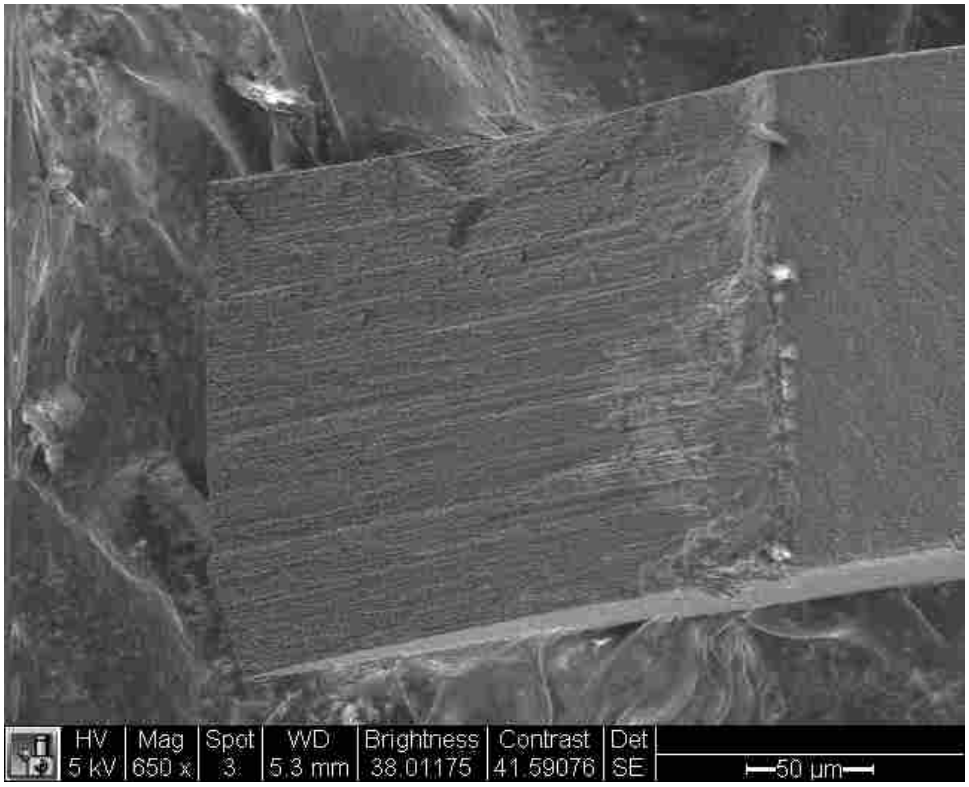

Figure 2.9: Uncapped CI-CNT Structure (Infiltrated for 45 mins at 850° C with hydrogen flowing at 311 sccm (0.0115 m/s)

being removed, a difference in infiltration level can be seen. Figure 2.10, which is the same sample imaged in Figure 2.8, shows nanotubes with an average thickness of about 68 nm based on the measurements taken, whereas in Figure 2.11, which is the same sample imaged in Figure 2.9, the nanotubes have an average thickness of about 121 nm based on the measurements taken. These images and measurements provide evidence that the samples infiltrated at 950° C are being capped off all around the outside of the beam at some point in the infiltration process, making it impossible for carbon to continue infiltrating the beam for the full 45 mins. This causes the nanotubes inside the beam to be thinner and farther apart, or for the beam to be less infiltrated with carbon, than the nanotubes inside the beam infiltrated at 850° C. The modulus of elasticity is still higher in this case for the beam infiltrated at 950° C most likely due to the full infiltration near the surface of the beam and the layer of solid carbon buildup surrounding the beam. However, it has lower strength due to its poor infiltration.

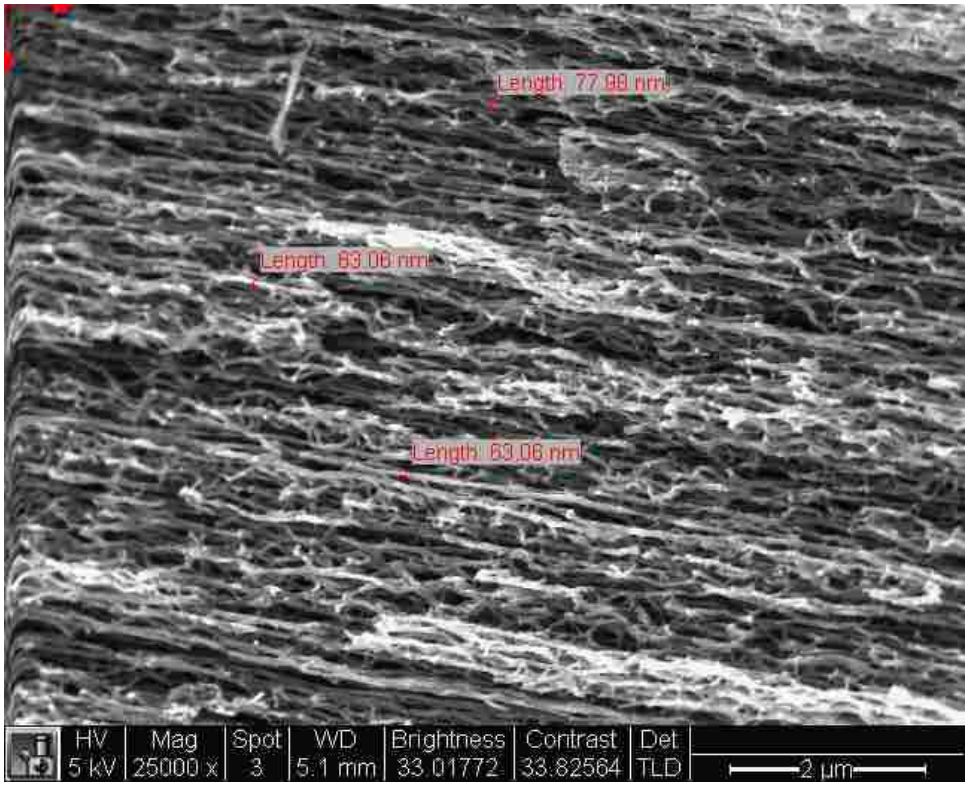

Figure 2.10: Capped CI-CNT Structure - Infiltrated for 45 mins at 950° C with hydrogen flowing at 311 sccm (0.0115 m/s) - Corresponds to Figure 2.8

2.3.3 Additional Experiment Data Based on Original Results

Based on the SEM images and on the trends in the data from Figure 2.6 another experiment was carried out using the same methods used in the previous experiments, but with an infiltration time of 150 mins at 850° C with a hydrogen flow rate of 311 sccm (0.0115 m/s). Figure 2.12 shows that the hypothesis that infiltrating at lower temperatures for longer periods of time does indeed increase the modulus of elasticity. Figure 2.13 shows that strength is also increased when infiltrating at lower temperatures for longer periods of time. These samples infiltrated at 850° C showed much higher stiffness and strength than any of the experiments from the initial experiment. With these parameters a modulus of 20.4 GPa and strength of 289.8 MPa were attained. The SEM image in Figure 2.14 shows that the beam is infiltrated to the point that it is difficult to pick out a single nanotube, or what would be considered completely infiltrated. The modulus and strength are much lower than those of amorphous carbon likely due to the voids that still exist in the infiltrated CI-CNT structures [22].

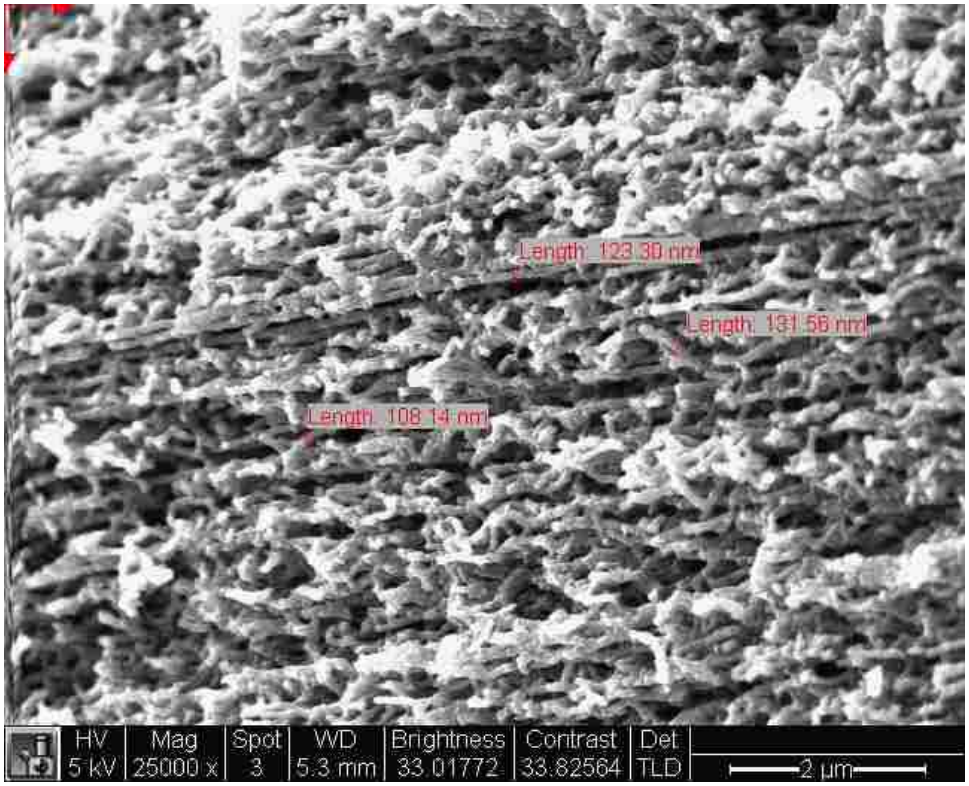

Figure 2.11: Uncapped CI-CNT Structure - Infiltrated for 45 mins at 850° C with hydrogen flowing at 311 sccm (0.0115 m/s) - Corresponds to Figure 2.9

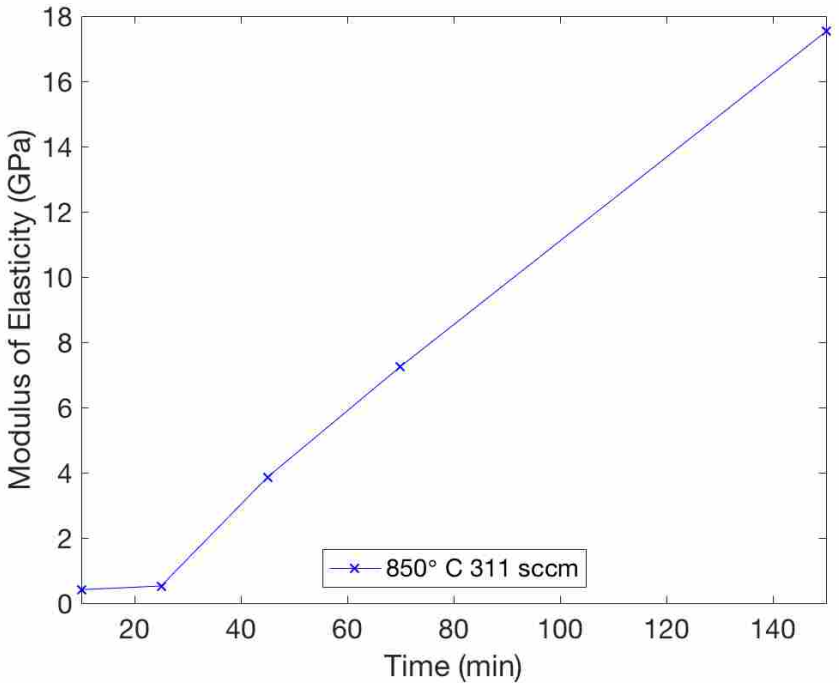

Figure 2.12: Modulus vs Time for expanded experiment at 850° C

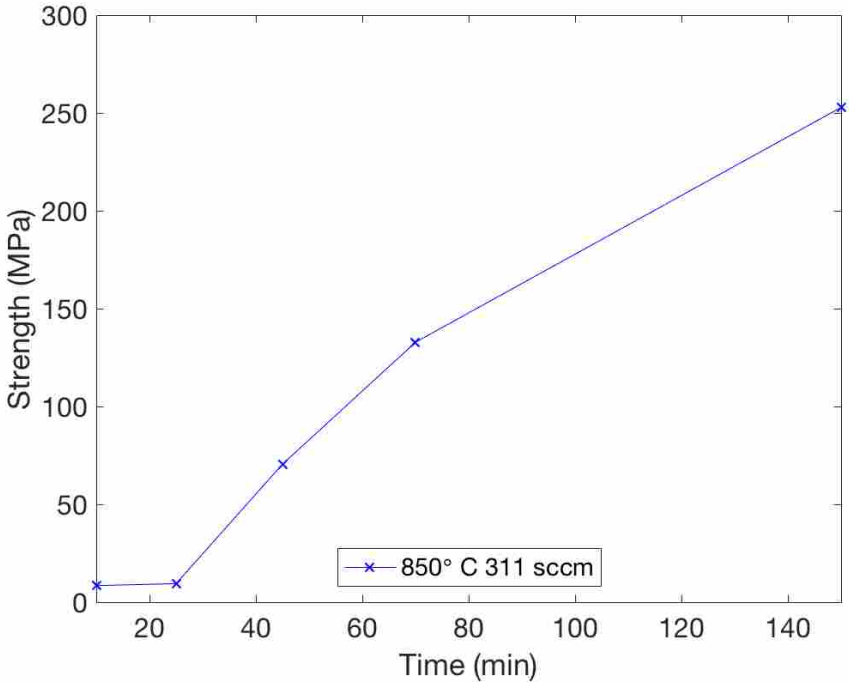

Figure 2.13: Strength vs Time for expanded experiment at 850° C and hydrogen flowing at 311 sccm

2.3.4 Correlations

From Figure 2.15 it can be seen that below about 500 kg/m^3 the modulus is less than around 1 GPa. After 500 kg/m^3 there is a strong trend that the higher the density, the higher the modulus. This can also be seen in Table 2.3, where the correlation coefficient between modulus and density is 0.828 with a p-value less than 0.001.

From Figure 2.16 it can also be seen that below about 500 kg/m^3 there is very low strength. However, after 500 kg/m^3 there is a strong trend that the higher the density, the higher the strength. This can also be seen in Table 2.3, where the correlation coefficient between strength and density is 0.827 with a p-value less than 0.001.

From Figure 2.17 it can be seen that there is a high correlation with the correlation coefficient between modulus and strength of 0.900 with a p-value of less than 0.001 as seen in Table 2.3. These plots further support the hypothesis that more complete filling of the space between the nanotubes leads to higher stiffness and strength. Hence, for best control of the material properties, it is important to infiltrate the CNT forest without capping, allowing a more even distribution of

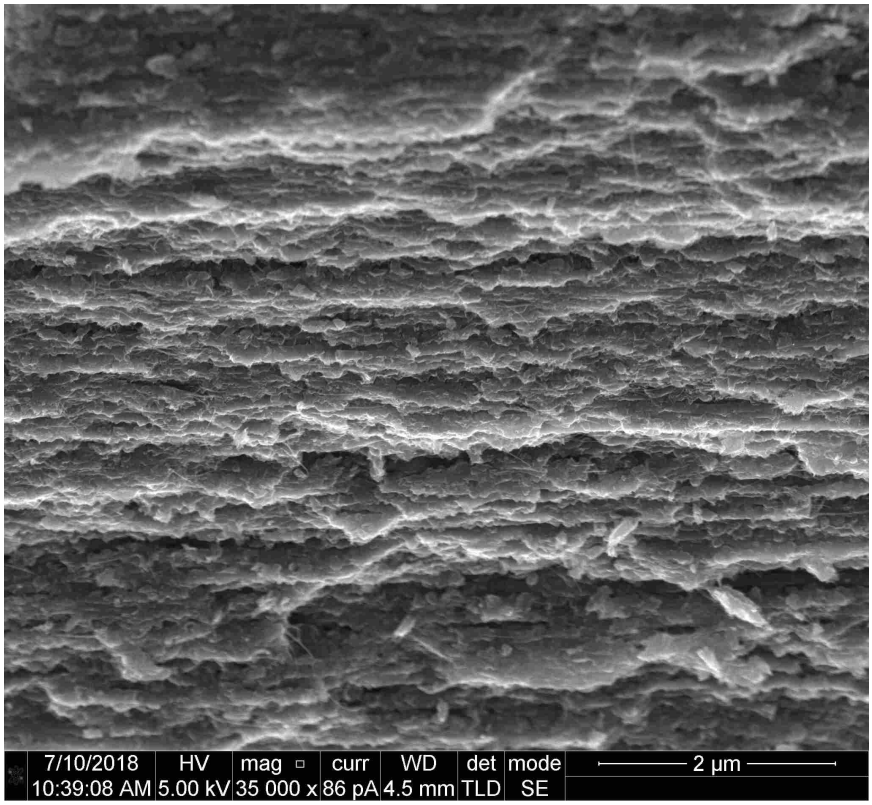

Figure 2.14: Completely infiltrated sample from expanded experiment at 850° C and hydrogen flowing at 311 sccm

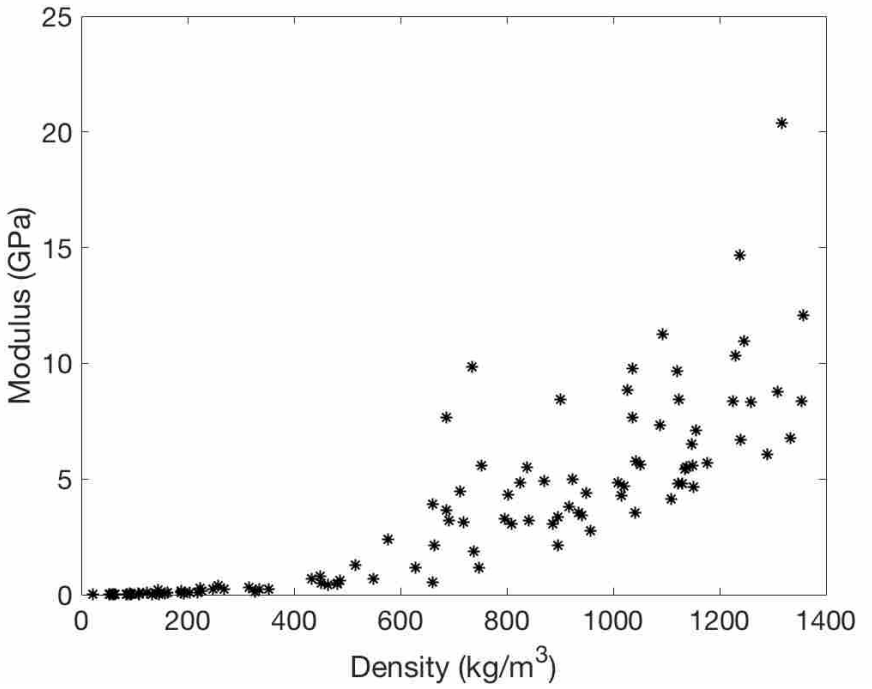

Figure 2.15: Modulus vs Density

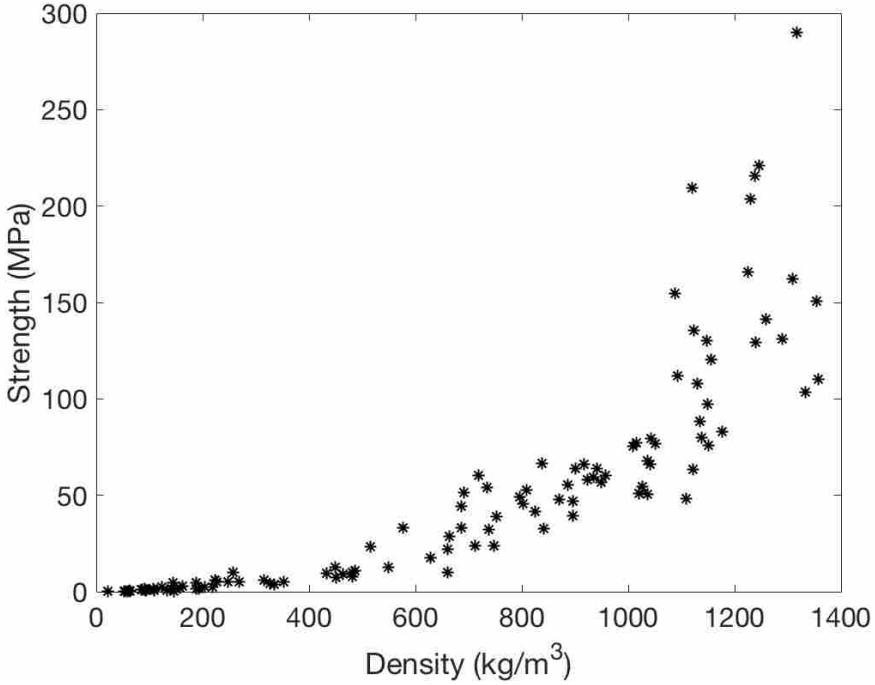

Figure 2.16: Density vs Strength

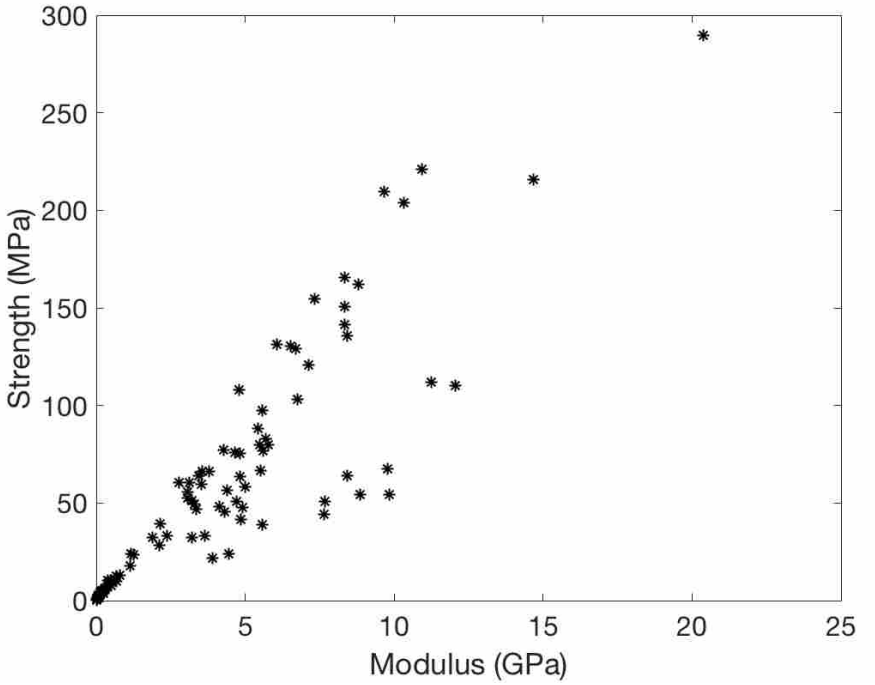

Figure 2.17: Modulus vs Strength

Table 2.3: Correlation Coefficients for Modulus of Elasticity, Strength, and Density with all p-values < 0.001 .

Correlations	Modulus of Elasticity	Strength	Density
Modulus of Elasticity	1		
Strength	0.900	1	
Density	0.828	0.827	1

infiltrated carbon throughout the cross section. This experiment suggests that infiltration at 850° C is an important parameter to achieve this effect.

CHAPTER 3. CONCLUSION

3.1 Best Practices for High Flexural Modulus and Strength

The data from the experiment suggests that the highest material properties of modulus and strength are achieved at lower temperature (850°) for a longer period of time (150 min). This is a new discovery as previous thinking and assumptions suggested that the highest strength and modulus were achieved at high temperatures (900°-950°) for shorter amounts of time (30-50 min). This research showed that at these elevated temperatures capping of the outside of the beams with a relatively thick carbon cap impedes infiltration of carbon further into the center of the structures. This causes these capped structures to be less solid than structures that are infiltrated for longer times at a lower temperature of 850° resulting in lower strength and modulus.

3.2 Tunable Material Properties

From the trends in the data gathered in the experiment it can be seen that for the highest modulus and strength are obtained using 850° C for the infiltration temperature for longer periods of time (70 min or more). This is because we found that 800° C is too low of a temperature for good infiltration and even after 70 min of infiltration these beams had a modulus of elasticity of less than 1 GPa and a strength of less than 10 MPa. From this data it is not recommended that 800° C be used for infiltration of MEMS devices. The data suggests that 900° C is a good temperature to use if your desired modulus is between 1 and 7 GPa and/or your desired strength is between 10 and 120 MPa. Using 311 sccm (0.0115 m/s) or 396.5 sccm (0.0146 m/s) as the hydrogen flow rate at 900° C brings these material properties to their maximums after only about 25 min. To get these same material properties using 850° C as the infiltration temperature it takes about 70 min using a hydrogen flow rate of 311 sccm (0.0115 m/s). For these desired properties 900° C infiltrations take only about a third of the time to infiltrate. However, if higher modulus than 7 GPa and higher

strength than 120 MPa are desired, then the data suggests that 850° C is the optimal temperature to use for infiltration. From the data from the SEM images it can be seen that this is due to the capping effect that occurs during the infiltrations of the beams at higher temperatures. This is especially evident with the beams infiltrated at 950° C with large amounts of carbon buildup surrounding the beam, even at lower infiltration times. At the lower temperature of 850° C it is believed that the infiltration occurs more slowly and evenly, and therefore this capping effect is slowed allowing the carbon to infiltrate deeper into the sample, but needing more time to do so. The data for infiltrating at 850° C for 150 min shows that much higher material properties for modulus and strength can be achieved, whereas at 900 or 950° C maximum strength and modulus due to infiltration have been reached by 70 min and any additional time only increases the properties due to the properties of the additional carbon buildup on the outside of the beams. The trend suggests that even higher values of material properties can be achieved at 850° C as there is a strong increasing trend in the data even after 150 min of infiltration.

The data shows that it is possible to tune the material properties of CI-CNT structures to the desired values for different designs or applications. This could be used for MEMS applications such as bistable mechanisms. By changing the material properties it would be possible to have different force requirements for switching for several such bistable devices with the same geometry. This could be very useful in manufacturing where one pattern or process could be used to make several devices with different characteristics. The only process that would change would be that of infiltration being tuned to the specific device requirements by changing the infiltration parameters with no need for changing geometry or the actual material selection of the device.

3.3 Non-destructive Material Property Estimation

From the collected data in Figure 2.15 and Figure 2.16 strong trends can be seen in increasing modulus and strength with increasing density. From these trends and data points it is possible to get a rough estimate of material properties by just finding the density of the CI-CNT device, rather than through destructive traditional material property testing. This method could also be used as a quality control check during manufacturing by being sure the density is within certain allowable tolerances for the desired particular material properties. It is also possible to estimate

material properties of modulus of elasticity or strength if either of the properties is already known using the data from Figure 2.17.

3.4 Possible Future Work

Work on uniform growth height would be of value. During this experiment there was a lot of variation at times in the height of the carbon nanotube forests. There are many different variables that could contribute to this including iron thickness, iron uniformity, amount of iron diffusion while waiting for nanotube growth and during the heating process before growth, gas purity, furnace cleanliness, and gas leakage in furnace tubing system to name a few. An in depth study of how these parameter affect the height of nanotube forest growth would be useful for better precision when making carbon nanotube MEMS devices.

Work on how geometry effects the material properties would also be of value. In this experiment only 0.2 mm width beams were used to determine the material properties, but knowing how geometry affects how infiltrated the sample are would be of interest as wider beams may not be infiltrated in the middle, away from the edges, which could greatly impact the effective modulus of elasticity and strength as seen in this work.

REFERENCES

[1] Hutchison, D. N., Aten, Q., Turner, B., Morrill, N., Howell, L. L., Jensen, B. D., Davis, R. C., and Vanfleet, R. R., 2009. "High aspect ratio microelectromechanical systems: A versatile approach using carbon nanotubes as a framework." In *TRANSDUCERS 2009 - 2009 International Solid-State Sensors, Actuators and Microsystems Conference*, pp. 1604–1607. 1

[2] Skousen, D. J., 2013. "Design Exploration and Analysis of Carbon- Infiltrated Carbon Nanotube Vascular Stents." Master's thesis, Brigham Young University. 1

[3] Toone, N. C., Fazio, W. C., Lund, J. M., Teichert, G. H., Jensen, B. D., Burnett, S. H., and Howell, L. L., 2014. "Investigation of unique carbon nanotube cell restraint compliant mechanisms." *Mechanics Based Design of Structures and Machines,* **42**(3), pp. 343–354. 1

[4] Qian, D., Wagner, G. J., Liu, W. K., Yu, M.-F., and Ruoff, R. S., 2002. "Mechanics of carbon nanotubes." *Applied Mechanics Reviews,* **55**(6), p. 495. 1

[5] Zhao, J., Li, Q., Gao, B., Wang, X., Zou, J., Cong, S., Zhang, X., Pan, Z., and Li, Q., 2016. "Vibration-assisted infiltration of nano-compounds to strengthen and functionalize carbon nanotube fibers." *Carbon,* **101**, pp. 114–119. 2

[6] Ding, J., Fu, S., Zhang, R., Boon, E., Lee, W., Fisher, F. T., and Yang, E.-H., 2017. "Graphene-evertically aligned carbon nanotube hybrid on pdms as stretchable electrodes." *Nanotechnology,* **28**(46), p. 465302. 2

[7] Li, A., Bogdanovich, A. E., Bradford, P. D., Lee, B. M., and Loh, K. J., 2017. "Carbon nanotube thin film strain sensors: comparison between experimental tests and numerical simulations." *IOP Publishing,* **28**(15), p. 155502. 2

[8] Lee, D., Hong, H. P., Lee, C. J., Park, C. W., and Min, N. K., 2011. "Microfabrication and characterization of spray-coated single-wall carbon nanotube film strain gauges." *Nanotechnology,* **22**(45), p. 455301. 2

[9] Robison, W. B., 2015. "A Study of Carbon Infiltrated Carbon Nanotubes Fabricated on Convex Cylindrical Substrates for the Creation of a Coronary Stent." Master's thesis, Brigham Young University. 2, 3

[10] Jones, K., Jensen, B. D., and Bowden, A., 2013. "Fabrication and Testing of Planar Stent Mesh Designs Using Carbon-Infiltrated Carbon Nanotubes." *Journal of Nanotechnology in Engineering and Medicine,* **4**(2), p. 020903. 2

[11] Stevens, K. A., Esplin, C. D., Davis, T. M., Butterfield, D. J., Ng, P. S., Bowden, A. E., Jensen, B. D., and Iverson, B. D., 2018. "Superhydrophobic, carbon-infiltrated carbon nanotubes

on Si and 316L stainless steel with tunable geometry." *Applied Physics Letters,* **112**(21), p. 211602. 2

[12] Barrett, L. K., Barton, D. J., Noyce, S. G., Allred, D. D., Vanfleet, R. R., and Davis, R. C., 2015. "High-aspect-ratio metal microfabrication by nickel electroplating of patterned carbon nanotube forests." *Journal of Microelectromechanical Systems,* **24**(5), Oct, pp. 1331–1337. 2

[13] Wang, J., Zhang, X., Miao, Y., Li, Y., Xi, X., Zhong, X., Pei, X., He, L., and Huang, Q., 2018. "The influences of carbon nanotubes introduced in three different phases of carbon fiber/pyrolytic carbon/silicon carbide composites on microstructure and properties of their composites." *Carbon,* **129**, pp. 409–414. 2

[14] Li, X., Tang, Y., Song, J., Yang, W., Wang, M., Zhu, C., Zhao, W., Zheng, J., and Lin, Y., 2018. "Self-supporting activated carbon/carbon nanotube/reduced graphene oxide flexible electrode for high performance supercapacitor." *Carbon,* **129**, pp. 236–244. 2

[15] Jensen, D. S., 2012. "Application of Carbon Nanotube Templated Thin Layer Chromatography Plates , and Functionalization of Porous Graphitic Carbon." PhD thesis, Brigham Young University. 2

[16] Fazio, W. C., Lund, J. M., Wood, T. S., Jensen, B. D., Davis, R. C., and Vanfleet, R. R., 2011. "Nanotube-Templated Structures for Microfabrication of." In *ASME 2011 International Mechanical Engineering Congress Exposition*, pp. 481–490. 2

[17] Hanna, B. H., Fazio, W. C., Tanner, J. D., Lund, J. M., Wood, T. S., Davis, R. C., Vanfleet, R. R., and Jensen, B. D., 2014. "Mechanical property measurement of carbon infiltrated carbon nanotube structures for compliant micromechanisms." *Journal of Microelectromechanical Systems,* **23**(6), pp. 1330–1339. 2

[18] Tao, J., Wang, K., Li, B., Liu, L., and Cai, Q., 2016. "Hierarchical models for the spatial-temporal carbon nanotube height variations." *International Journal of Production Research,* **54**(21), pp. 6613–6632. 3

[19] Fazio, W. C., 2012. "Mechanical Properties and MEMS Applications of Carbon-Infiltrated Carbon Nanotube Forests." Master's thesis, Brigham Young University. 5

[20] Moulton, K., Morrill, N. B., Konneker, A. M., Jensen, B. D., Vanfleet, R. R., Allred, D. D., and Davis, R. C., 2012. "Effect of iron catalyst thickness on vertically aligned carbon nanotube forest straightness for CNT-MEMS." *Journal of Micromechanics and Microengineering,* **22**(5), p. 055004. 5

[21] Richard G. Budyanas, J. K. N., 2011. *Shigley's Mechanical Engineering Design*. McGraw-Hill. 10

[22] Cho, S., Chasiotis, I., Friedmann, T. A., and Sullivan, J. P., 2005. "Young's modulus, poisson's ratio and failure properties of tetrahedral amorphous diamond-like carbon for mems devices." *Journal of Micromechanics and Microengineering,* **15**(4), p. 728. 17